Characterisation of R.F. magnetron sputtered Cr-N, Cr-Zr-N and Zr-N coatings

Mamoun Fellah, Linda Aissani, Mohamed Abdul Samad, Said Mechacheti, Mohamed Zine Touhami, Alex Montagne, Alain Iost

Characterisation of R.F. magnetron sputtered Cr-N, Cr-Zr-N and Zr-N coatings

Mamoun Fellah*[1,2], Linda Aissani[2,3], Mohammed Abdul Samad[4], Said Mechacheti[5], Mohamed Zine Touhami[5], Alex Montagne[6] and Alain Iost[6]

Binary Cr-N, Zr-N and Cr-Zr-N films were synthesised using a R.F. reactive magnetron sputtering technique by co-sputtering Cr and Zr. The crystalline structure, morphology, mechanical and tribological properties of the films as a function of Zr content were characterised by X-ray diffraction, microanalysis X (WDS, EDS), X-ray photoelectron spectroscopy, scanning electron microscopy, atomic force microscopy, nanoindentation, scratch adhesion and pin-on-disc sliding wear tests. The residual stress was calculated with the Stoney formula. The Cr-Zr-N films exhibit a two-phase microstructure, containing a cubic (CrN, ZrN) with hexagonal (Cr_2N, Zr_2N) phases, as shown by X-ray diffraction. As the Zr content increased, a columnar and compact structure is developed with a low surface roughness. The results reveal that the mechanical and tribological properties of the films were found to depend on the Zr content and the hardness (maximum 26.3 GPa) is greatly improved in comparison with CrN and ZrN films, especially at 31 at.-% Zr. In the scratch test, the hardest film ($Cr_{0.18}Zr_{0.31}N_{0.47}$) exhibited an adhesive failure at $Lc_2 = 34.3$ N.

Keywords: RF magnetron sputtered coatings; CrN; ZrN; Cr-Zr-N; Ternary chromium alloy; Hardness; Wear properties

Introduction

CrN films are among the most extensively studied and frequently used films in different industrial applications such as diffusion barriers in micro-electronics, wear resistant coatings on cutting tools, optical, mechanical and tribological devices due its low friction coefficient, high surface hardness and high toughness, as compared to other transition metal nitrides such as TiN.[1,2] However, in spite of its excellent properties, CrN is not suitable for many demanding applications such as high speed machining and applications operating at high temperature conditions due to the limitations of its binary system.[3] For this reason, a ternary nitride system with the addition of other elements into the Cr-N system is presently being explored by researchers.[1–4] Depending on the chemical properties of the deposited elements and the process parameters, the addition of transition metals and the formation of new nanocomposite materials or solid solutions such as Cr-Ti-N,[4] Cr-Al-N[5] and Cr-Zr-N[3] significantly improved the mechanical and tribological properties of CrN coatings. This improvement in the CrN properties attracted a lot of industrial interest and hence has been explored in several significant studies. These new compounds were developed and their excellent properties such as high oxidation resistance and very low surface roughness as compared to the Cr-N system have been widely reported.[3] In particular, Zr, which shows an excellent behaviour in mixtures with metallic[3] or nonmetallic elements,[6] when added to CrN resulted in a significant improvement in the structure, mechanical/wear properties and also in the surface roughness of the films.[3] Also, the ternary Cr-Zr-N compounds give rise to the opportunity to adjust parameters such as lattice constant, thermal expansion and stability against corrosion, in order to further enhance the performance of the Cr-N coatings. However, only a few studies have been devoted to the Cr-Zr-N system.[3] Hence the focus of the present study has been to characterise the thin Cr-Zr-N films deposited by the R.F. reactive magnetron sputtering system by co-sputtering of Cr and Zr and evaluate the structural, mechanical and tribological properties of these coatings as a function of Zr content.

[1]Mechanical Engineering Department, ABBES Laghrour – Khenchela University, P.O 1252, 40004, Algeria
[2]Materials, Tribology, Surface and Interfaces Group, Laboratory of Foundry, Annaba University BO, 12 CP 23000, Algeria
[3]Physics Department, ABBES Laghrour – Khenchela University, P.O 1252, 40004, Algeria
[4]Mechanical Engineering Department, King Fahd University of Petroleum & Minerals, Box 1180, Dhahran 31261, KSA
[5]Laboratory of Foundery, University of Annaba, P.O 12, Annaba 23000, Algeria
[6]Mechanical Surfaces and Materials Processing Laboratory, ENSAM Arts et métiers Paris Tech 8 Boulevard Louis XIV, 59800 Lille, France

*For correspondence: mamoun.fellah@yahoo.fr

Experimental details

Cr-N, Zr-N and Cr-Zr-N thin films were deposited at a total working pressure of 0.4 Pa using a R.F. magnetron sputtering system (NORDIKO type 3500, 13.56 MHz, 1.25 kW) with a base pressure of 2×10^{-5} Pa with a purity (0.3:Ar (99.99%) + 0.1:N_2 (99.99%)). Two separate target

Table 1 Pressure (*P*), voltage (*V*), applied power (*P*), Ar:N_2 ratio, temperature (*T*) and deposition time (*t*) of the CrN, Cr-Zr-N, and ZrN films

	Gas		Cr		Zr			
Film	P/Pa	Ar:N_2	P/W	U/-V	P/W	U/-V	*T*/°C	*t*/min
CrN	0.4	0.3/0.1	650	900	…	…	200–150	90
$Cr_{0.44}Zr_{0.7}N_{0.47}$			650	900	250	300		
$Cr_{0.18}Zr_{0.31}N_{0.47}$			550	700	630	900		
$Cr_{0.10}Zr_{0.42}N_{0.47}$			260	300	630	900		
ZrN			…	…	630	900		

discs of diameters 10.16 cm each (purity of 99.99% for Cr and 99.98% for Zr) were used with a substrate to target distance of 80 mm and at an angle of +45° (Cr) and −45° (Zr) from the normal for all depositions, to obtain films of uniform thickness at a good deposition rate. The films were deposited onto Si (100) (10×10 mm², 380 µm thick) wafers and XC 100 steel substrates discs (15 mm diameter, 3 mm thick) at 200°C for 90 min. The specific details of the deposition conditions used in this work have been reported earlier.[1,7]

The chemical composition of XC 100 steel substrate is: (0.95–1.05) wt-% C, (0.5–0.8) wt-% Mn, 0.25 wt-% Si, 0.05 wt-% S, 0.035 wt-% (P and S), the balance being Fe. The substrates were ground, polished and ultrasonically cleaned for 5 min (each successively in trichloroethylene, methanol and acetone) to a roughness (Ra) of approximately 0.03 µm (measured by atomic force microscopy). Before deposition, the substrates were etched under Ar^+ ions bombardment for 5 min at −700 V (350 W) and at 0.1 Pa. The targets were also cleaned under an Ar^+ discharge for 5 min, at −500 V (250 W) and 0.4 Pa before deposition. A thin layer of about 200 nm thick was used as a sublayer in order to improve the adhesion of the coatings to the substrate. The Cr-Zr-N thin films were deposited under varying Cr and Zr voltages (target power) from 0 to −900 V (0–650 W) with N_2/Ar ratio of 0.25. The Cr and Zr power and voltage values are shown in Table 1.

The film density was calculated from the mass (Sartorius microbalance),[1] the crystalline structure, lattice parameters (Bragg's equation) and crystallite size (Scherer's equation)[8] of all these deposited films were determined via a $\theta/2\theta$ X-ray diffractometer (SIEMENS, D500) with a Bragg–Brentano geometry using CoK_α radiation ($\lambda_{Co} = 0.178$ nm) and operated at 40 kV and 40 mA. The step size was 0.05° 2θ with 0.02 s per step. The film thickness, surface morphology and fracture cross-sections of the coatings were examined with a scanning electron microscope (SEM, JEOL JSM-5900LV). Film composition was determined by microanalysis X (WDS, EDS, Oxford INCA x-act), which was attached to the scanning electron microscope, and X-ray photoelectron spectroscopy, with voltages of 5 and 15 kV in order to locate the interaction volume of 300 nm thickness. The analysis error of the oxygen content was estimated to be about 1 at.-% and that of Cr, N and Zr could reach up to 5 at.-%. (XPS, Riber SIA 100); the XPS chemical composition was estimated from the area under the peaks of the core level: N1s, Cr2p, Zr3d and O1s. The surface roughness of the coating was examined using an atomic force microscope (AFM 100, APE Research).

Hardness and Young's modulus were measured by means of a nano-indentation tester (MTS XP nano-indenter). A continuous stiffness measurement (CSM) mode was used and tip oscillating with a frequency of 45 Hz and amplitude of 2 nm was used. A diamond Berkovich indenter with a tip radius of about 200 nm was used in the experiments with a maximum load of 10 mN. The loading and unloading phases of the indentations were carried out under load control at a nominal rate of 0.05 mN s^{-1}. The compressive residual stresses (σ) of the films were calculated using Stoney's equation.[11]

The tribological properties were evaluated by using a pin-on-disk configuration using an oscillating (TRIBO tester) wear test at a room temperature of 23.5°C and a relative humidity of 38.2%. A 100Cr6 ball with a diameter of 6 mm, hardness of 700 $HV_{0.2}$ was used as counter face under a constant normal load of 5 N and a constant sliding speed of 0.5 mm s^{-1}. The friction coefficient was determined after a sliding distance of 0.3 m for 10 min.

The film adhesion was evaluated by means of scratch tests (Scratch Tester Millennium 200). The tests were carried out using a Rockwell diamond indenter (diameter, radius and conical angle of 0.2 mm, 200 µm and 120°, respectively). The scratch speed and length were 3 mm min^{-1} and 8 mm, respectively. After the scratch tests, scanning electron microscopy and microanalysis X was used to evaluate the wear scars.

Results and discussion

Structural characterisation

The structures of Cr-N, Zr-N, Cr-Zr-N coatings deposited at different Cr and Zr contents by various sputtering powers (Table 1) on XC 100 substrates were analysed by XRD, and the atomic concentrations of Cr, Zr, N and O on Si substrates were determined by microanalysis X and XPS analysis. The results are listed in Table 2 and presented in Figs. 1 and 2, respectively.

It is to be noted that the presence of CrN phase in the films can be detected by the presence of (111), (200) and (220) and (311) peaks corresponding to the fcc structure of CrN as observed by Twu *et al.*[9] for R.F. reactive magnetron sputtering of CrN coating. Also, CrN coatings prepared by triode sputtering magnetron at different nitrogen partial pressures, exhibited a strong CrN (111) preferred signal with a small CrN (200) signal as seen by Pradhan *et al.*[10] In this work, the Cr-N coating results in a N/Cr atomic ratio of 0.96, and is comparable to the chemical composition data from CrN films deposited by using the same method which is characteristic of the NaCl cubic CrN phase.[10–12] As can be seen from Fig. 1, the XRD analysis shows oriented cubic CrN phase corresponding to (111) and (200) planes (JCPDF 01 0065) and hexagonal Cr_2N phase corresponding to (111) and (200)

Table 2 Atomic concentration/at.-% and thickness/μm, lattice parameter and crystallite size of CrN, Cr-Zr-N, and ZrN films

Properties		Film				
		Cr-N	$Cr_{0.44}Zr_{0.7}N_{0.47}$	$Cr_{0.18}Zr_{0.31}N_{0.47}$	$Cr_{0.13}Zr_{0.39}N_{0.47}$	Zr-N
Chemical composition at.-%	N	47.8	47.4	47.3	46.4	47.4
	Cr	50.0	43.6	18.3	12.7	…
	O	2.2	2.0	2.6	2.3	3.8
	Zr	…	7.0	28.8	39.6	48.8
	N/(Cr + Zr)	0.96	0.94	0.95	0.94	0.97
Structural parameters	Thickness e/μm	1.26	1.48	1.74	2.05	1.28
	Grain size L/nm (±0.5)	15.8	12.5	8.3	19.1	19.6
	Lattice P. a/nm CrN (111) (±0.005)	0.417	0.422	0.424	0.424	–
	Lattice P. a/nm ZrN (200) (±0.005)	…	…	…	0.461	0.462
	Density (±0.05)	5.78	5.67	5.66	5.66	7.15

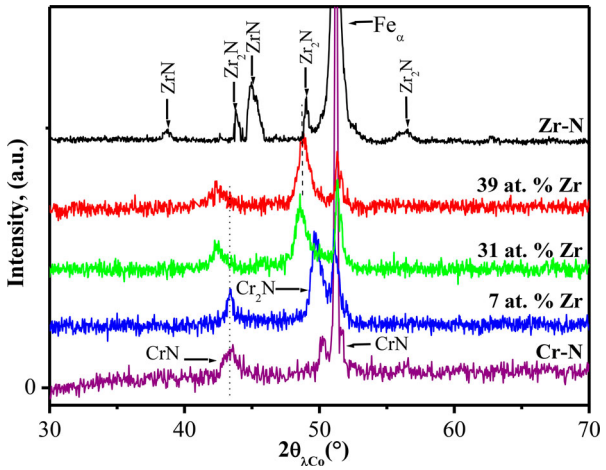

1 XRD patterns for: Cr-N, Cr-Zr-N and Zr-N films

planes (JCPDF 35 0803), which is attributed to the formation of CrN and Cr_2N mixtures, as has been previously reported by other authors.[8,10]

A lattice parameter and a density of 0.417 ± 0.005 nm and 5.78 ± 0.05 g cm^{-3}, respectively, were calculated by taking the average of the lattice parameters calculated from (111) diffraction peak. The positive deviation of 2θ planes position and the increase of lattice parameter (Table 1), when compared to CrN theoretical values of 0.4140 nm and 5.9 g cm^{-3} (JCPDF 01 0065), indicates a compressive residual stress and a variation of Cr interstitial sites during the nitrogen diffusion.[8,12] The crystallite size calculated from the (111) plane is approximately 15.8 ± 0.5 nm.

A series of Cr-Zr-N samples with different compositions were deposited at different Cr and Zr contents. The compositions are as follows: $Cr_{0.44}Zr_{0.7}N_{0.47}$, $Cr_{0.18}Zr_{0.31}N_{0.47}$ and $Cr_{0.13}Zr_{0.39}N_{0.47}$.The addition of Zr slightly reduced the N/(Cr + Zr) ratios (0.94–0.97) with an increase in Zr/Cr ratio. At 7 at.-% of Zr, the Cr/N atomic ratio decreases as compared to that of CrN coatings, which can be attributed to the formation of Cr_2N and CrN mixture structures and a good correspondence, can be observed from the XRD spectra. The XRD spectra showed a strong (111) peak of the hexagonal Cr_2N phase along with a small peak of CrN (111). The coating showed a lattice constant and a density of 0.424 ± 0.005 nm and 5.67 ± 0.05 g cm^{-3}, respectively, which is slightly greater than that of the CrN film (0.41 nm) and the bulk CrN phase (JCPDS 001 65). At between 31 and 39 at.-% of Zr, random orientations were detected. The Cr-Zr-N films exhibited (111) orientation of CrN, (200) of ZrN (JCPDS 02 0956), (111) and (200) of Zr_2N (JCPDS 46 1204). This indicates that the structure is denser than that seen for pure CrN film. In addition, the position of the CrN (111) peak monotonously shifts towards the lower (2θ) diffraction angles with increasing Zr content in the films. This may be explained through a number of reasons such as the entering of the excess N atoms in the crystal lattice which changes the lattice constants, the presence of compressive stresses and the dense structure by increasing of the ion bombardment energy during the deposition process especially for the PVD Cr-Zr-N films.[3] This behaviour was also observed for Cr-Mo-N, Cr-Ti-N and Cr-Nb-N films.[12] On the other hand, it is observed that the intensity of (111) CrN peak is considerably reduced with increasing Zr content in the Cr-Zr-N system. However, (200) Cr_2N orientation is detected in each film starting from 31 at.-% Zr. The lattice constants (Table 2) increase steadily as the content of Zr increases. This indicates that increasing the Zr/Cr ratio causes more Zr ions to occupy the sites of the Cr, because the Zr atom ions are bigger in size than the Cr ions. A similar result was observed in the Cr-Zr-N films synthesised by closed field unbalanced magnetron sputtering with vertical magnetron sources by Chantharangsi *et al.*[13] These results suggest that the lattice structure of Cr-Zr-N films synthesised in this study forms a new solid solution whereby Cr atoms are substituted by Zr. An increase of lattice parameter is observed by a decrease in the N content of the CrN resulting in an initial increase in lattice parameter which is confirmed by a decrease in the N/Cr atomic ratio. A similar result was observed in the Zr-C phase by Katoh *et al.*[6] The crystallite size, as determined from the XRD peaks, decreases from 15.8 ± 0.5 to 8.3 ± 0.5 nm with a significant correlation with the increase of Zr/Cr ratio in the Cr-Zr-N films.

The Zr-N coating was composed of a mixture of Zr_2N and ZrN phases and showed a N/Zr atomic ratio of around 0.97 according to microanalysis X analyses. The XRD spectrum of the ZrN film showed that the films were composed of well-crystallised ZrN (200) phase with low intensity peaks of (111) ZrN (JCPDS 002 0956) and (111) (200), and (121) Zr_2N peaks, respectively (JCPDS 046 1204). This structure was also observed by Pelleg *et al.*[14] and Oh *et al.*[15] The ZrN preferred

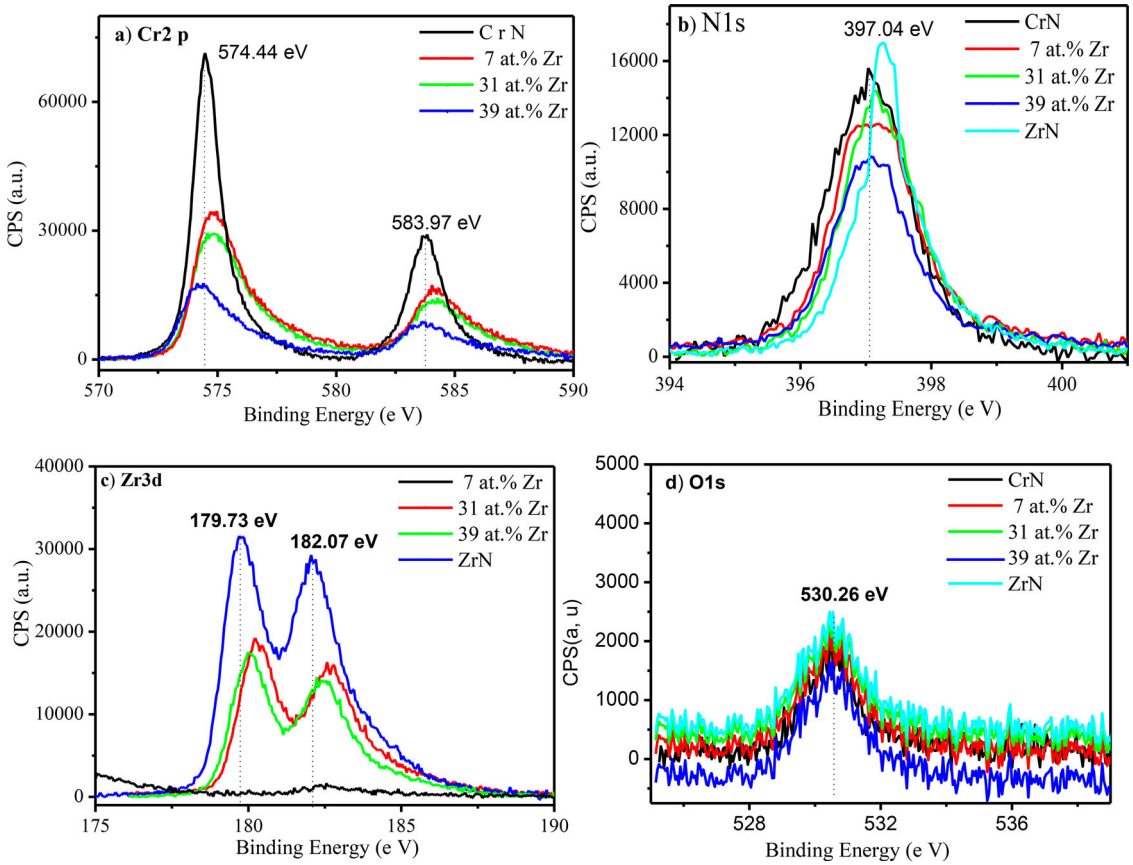

2 XPS spectra for Cr-N, Cr-Zr-N and Zr-N films

orientation is determined by the competition between two thermodynamic parameters, the free surface energy and the strain energy. The lattice parameter and density of ZrN film are 0.462 ± 0.005 nm and 7.15 ± 0.05 g cm^{-3}, respectively, and which was calculated by the ZrN (111) plane and is greater than that calculated for bulk ZrN phase (0.458 nm, 7.09 g cm^{-3}, JCPDS 002 0956). This difference can be attributed to several different effects including selective entrapment of interstitial nitrogen atoms and growth of lattice defects during ZrN film deposition.[14] These effects are marked as a shift of 2θ angles position to lower values and a significant strain in the ZrN lattice parameter ($\sigma_{ZrN} = -1.96$ GPa). The crystallite size calculated from the ZrN (111) plane is approximately 19.6 ± 0.5 nm. The variable lattice parameter, the density, the film composition and Cr + Zr/N ratio with increasing Zr content were correlated with film density and the film roughness.[6] Nevertheless, the stoichiometry of Cr-N, Zr-N and Cr-Zr-N films is not entirely reached because of residual oxygen which is about 2–3.8 at.-%, mainly located in the film and which partly replaces the nitrogen. This oxide probably originates from oxidation when the samples were removed from the vacuum chamber and from the residual oxygen in the sputtering gas.[10]

Figure 2 shows the XPS spectra of N 1s, Cr 2p, Zr 3d and O1s for each of the Cr-Zr-N films with different Cr to Zr ratios. For a pure Cr-N film, the N 1s spectrum shows a single wide peak at 397.1 eV (Fig. 2*a*). This value indicated that the CrN is formed and gives additional evidence to support the bonding of N to Cr during the coating deposition.[16,17] The Cr ($2p_{1/2}$, $2p_{3/2}$) peaks are composed of spin–orbit doublets, with a separation of 9.6 eV; corresponding to binding energies of 574.40 and 584.79 eV, respectively (Fig. 2*b*). According to Conde *et al.*,[16] the peaks correspond to the Cr–N bonds in the Cr-N film. The XPS results are in very good agreement with XRD analysis. For the Cr-Zr-N films, N1s peaks show almost the same tendency for the three coatings with the binding energies in the range of 397.1–397.2 eV (Fig. 2*b–d*). However, their intensities are slightly varied, where the sample with lower Zr content (7 at-%) shows a lower intensity compared to the intermediate (31 at-%) and the higher content Zr samples (39 at-%), which is indicative of a changed growth mode. For Cr 2p, XPS band measurements revealed a progressively negative shift from 574.80, 584.23 eV for 7 and 31 at.-% Zr down to 574.47, 584.22 eV for 42 at-% Zr (Fig. 2*b*). A gradual decrease in the Cr2p peak intensity is also observed in Cr-Zr-N films with increasing Zr content, suggesting a change in the nature of the Cr bond from a Cr–N[15] to a pure metallic Cr–Cr.[18] These results suggest the gradual transformation of CrN to Cr_2N and the formation of Cr-Zr-N solid solution.[17,19] It is also observed that the Zr 3d ($3d_{5/2}$, $3d_{3/2}$) XPS peaks are composed of spin–orbit doublets, with a separation of 2.3 eV and a slight chemical shift to the higher binding energy with an increase in the Zr content (Fig. 2*c*). The peaks shifted from 180.22, 182.62 eV at 31 at-% of Zr, to 180.03, 182.43 eV at 39% of Zr, respectively. These peak positions correspond to the Zr-N band as observed in an earlier study.[20] This kind of Zr3d peaks shift as compared to what has been observed for stoichiometric ZrN[21] is due to the non-stoichiometry of Cr-Zr-N films due to the decrease in the nitrogen content.[22] At 7 at-% Zr, the Zr3d peaks did not give any information because

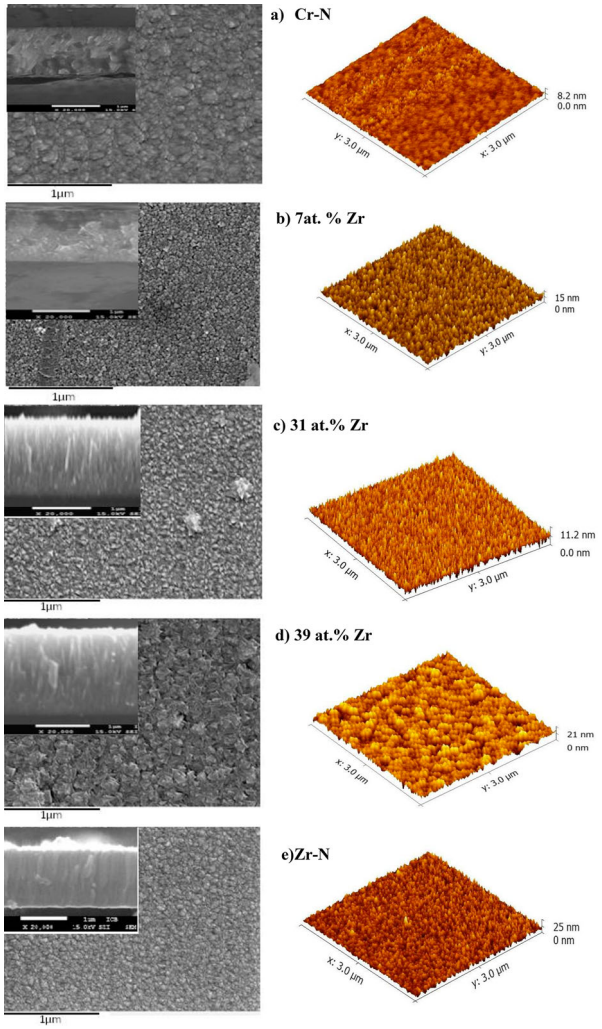

3 SEM cross-sections and surface morphologies for Cr-N, Cr-Zr-N and Zr-N films

of the lower Zr concentration in the film. It can be observed that for the Zr-N film, the Zr3d, and N1s peaks were found to be located at 179.3, 182.62 and 397.3 eV, respectively. The peaks corresponding to these binding energies can be ascribed to Zr-N bonding. The oxygen peaks in the XPS spectrum for the films were observed at a binding energy of about 531.2 eV which can be attributed to the surface contamination of the films (Fig. 2*d*).

The surface morphology, the fractured cross-section and the corresponding roughness (Ra, obtained by AFM) are displayed in Fig. 3. The Cr-N coating shows a compact columnar structure with a roughness of about 15.8 ± 0.1 nm (Fig. 3*a*). This aspect is observed when the coating is in a compressive stress state.[21] Additionally, this coating displays a small grain size without micro-droplets or craters in the surface morphology as a result of the mutual interference of the intermediate CrN and Cr_2N phases.[22] The CrN coating thickness was found to be about 1.26 µm. It is observed that the developed film structure belongs to the structure of zone II, in agreement with the structural model zones proposed by Mahieu *et al.*[23] Similar morphology evolution has also been reported in the literature.[21,22]

With an increasing Zr content from 7 to 31 at.-% Zr, the Cr-Zr-N films shows a smooth and columnar growth with a RMS roughness value ranging from 11.3 ± 0.1 to 15.1 ± 0.1 nm (Fig. 3*b* and *c*). This structure is related to the multi-component coatings as reported by other researchers.[24] Thus, with an increase in the Zr content, the grain size decreased and the film thickness increased due to the continuous re-nucleation and the formation of a nanocomposite structure which favours grain refinement during the growth process. Similar grain size variation with different Zr and Cr contents was observed in Cr-Zr-N films by Aouadi *et al.*[22] According to the Mahieu SMZ,[23] this structure is between zone I-a and zone I-b. As the Zr content increases to 39 at.-%, a mixture of round and faceted grains are found on the surface without defects (Fig. 3*d*), indicating the presence of a random structure with the apparition of (111) Cr_2N and (002) Zr_2N peaks. But, the RMS roughness shows a significant increase of 21.0 ± 0.1 nm which may be related to the increase in the film thickness, the formation of new structure composite and the competitive growth between Cr_2N and CrN.[8,25] The Zr-N coating also reveals a compact columnar structure with a small grain size (Fig. 3*e*). The Zr-N coating exhibited low thickness and higher RMS roughness, 1.28 µm, 25.1 ± 0.1 nm, as compared to Cr-N and Cr-Zr-N films. According to Mahieu *et al.*[23] this structure is compatible with zone II. This structure is similar to that of Zr-N films grown by PVD techniques at low substrate temperatures.[26]

Mechanical properties

Figure 4 shows the variation of hardness, Young's modulus and residual stress of Cr-Zr-N films as a function of Zr content. The variation of hardness according to the different Zr content follows closely the same trend as the Young's modulus (Fig. 4).[8] The hardness and Young's modulus of the Cr-N coating are 19.53 ± 0.11 GPa and 287.91 ± 25.11 GPa, respectively. These values are in good agreement with those reported for CrN film deposited by different methods.[11,27,28] On the other hand, the Zr-N film exhibits a hardness value of 16.00 ± 0.10 GPa and Young's modulus of 270 ± 23.00 GPa. The ZrN hardness value is comparable to those reported in the literature which range from 15 to 30 GPa for bulk ZrN phase[29] and also in good agreement with that reported for films grown by PVD techniques. However, the ZrN Young's modulus observed in the present study is lower, suggesting that the Young's modulus of the ZrN (200) plane might be lower than that of ZrN (111) planes.[28] The reason for the high hardness of binary Cr-N and Zr-N coating is found in the small grain sizes, 15.80 ± 0.50 nm (CrN) and 19.60 ± 0.40 nm (ZrN), the presence of hexagonal Cr_2N and Zr_2N phases, detected by XRD, whose hardness are higher when compared to coatings with dominant CrN and ZrN phases and also of the compressive residual stress states of the films, which are −1.98 ± 0.05 GPa for Cr-N and −196.00 ± 12.00 GPa for Zr-N. The hardness shows a definite maximum of 26.30 ± 0.11 GPa for the $Cr_{0.18}Zr_{0.31}N_{0.47}$ coating.

The $Cr_{0.13}Zr_{0.39}N_{0.47}$ exhibits a slightly lower hardness of 15.00 ± 0.10 GPa, whereas, the Young's modulus essentially displays a simple decline with increasing of the Zr content. A similar hardening tendency was observed in Cr-Zr-N films deposited by unbalanced magnetron dc sputtering technique for $Cr_{11}Zr_{44}N_{45}$ as reported by Aouadi *et al.*[22] and Cr-Ti-N films deposited

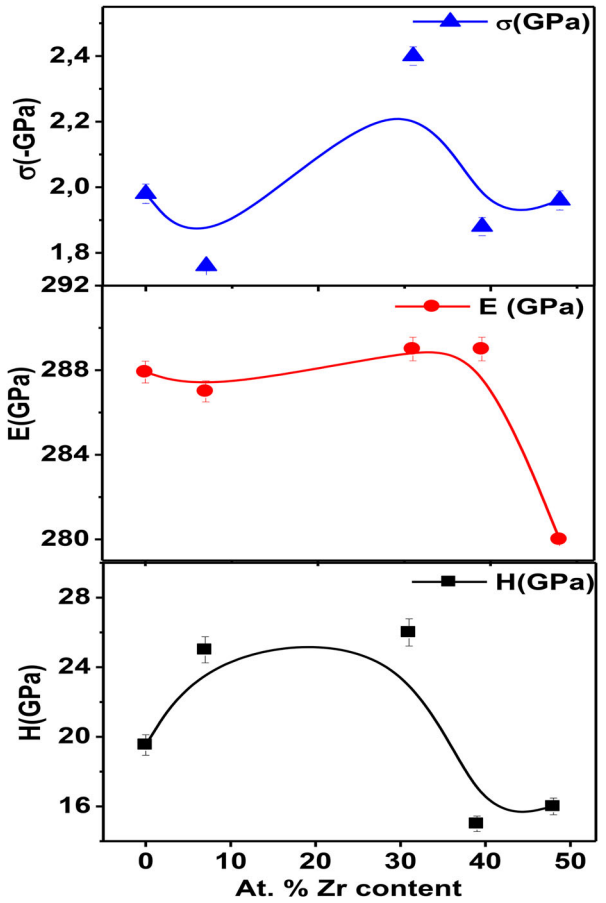

4 Hardness, Young's modulus and residual stress for Cr-N, Cr-Zr-N and Zr-N films

by unbalanced multi-targets reactive magnetron sputtering for $Cr_{32.5}Ti_{24.6}N_{42.9}$ phase.[4] The improvement of mechanical properties in Cr-Zr-N films cannot be easily explained because they are the result of complex influences of the chemical and physical properties, the growth mode, the film morphology and the stress state. Kim *et al.*[3] has reported that the hardness increases with increasing Zr content in the Cr-Zr-N films by the formation of the hardening solid solution which inhibits the mobility of the dislocations by the distortion of the CrN lattice parameter with Zr insertion in the film. Aouadi *et al.*[22] explained the improvement in the mechanical properties of the Cr-Zr-N films by the formation of a nanocomposite structure and the reduction of grain size. In the present study, the grain size (through the Hall–Petch hardening effect) can be considered as a major factor because there is a significant reduction in the grain size as the films become denser, as deduced from the XRD and SEM analyses.

The crystallite orientation in Cr-Zr-N films changes from CrN (111) preferred peak to random orientation ((111), (111) and (200) ZrN and (111) Zr_2N as detected by XRD) which can also contribute to the increase of hardness by creating a large number of grain interfaces. These interfaces can hinder the propagation of dislocations along the predominant CrN (111) plane and the other planes.[30] On the other hand, the presence of a strong mixture of Cr–N and Zr–N phases, which have higher hardness and Young's modulus, may contribute to the increase in the Cr-Zr-N coatings hardness.[31] Moreover the presence of hexagonal Cr_2N phase, which is harder when compared to the cubic CrN phase, may also significantly contribute to the increase in the hardness of the Cr-Zr-N coatings.[31,32]

According to XPS analysis, the peak shifts in Cr2p binding energy suggests that the bonding character changes from the Cr-N to the Cr–Cr bonds due to the charge transfer from nitrogen to Cr atoms as a function of Zr content. This shows that Zr-containing films exhibit a higher covalence level than pure CrN, which could account for the hardness increase. A similar correlation is also observed in Cr-Ti-N[4] and Cr-Ni-N thin films.[33] The residual stress follows the same trend as hardness with varying Zr/Cr ratio,[34] which showed a small increase from -1.76 ± 0.11 GPa at 7 at.-% Zr to -2.04 ± 0.09 GPa at 31 at.-% Zr (Fig. 4) and approaches that of pure CrN at 39 at.-% Zr which is -1.88 ± 0.12 GPa. This may be due to the incident energetic particles affecting surfaces during the deposition of the film and the incorporation of Zr atoms into the interstitial nitrogen sites.[35] The residual stress reduction can be considered the reason for the decrease in hardness at 39 at.-% Zr.

Tribological properties

Figure 5 shows the friction coefficient and RMS roughness variation of coatings with different Zr contents. The friction coefficient of the binary Cr-N and Zr-N is 0.55 and 0.60, respectively. For the Cr-Zr-N, the friction coefficient and RMS roughness takes a minimum of 0.42 and 7.1 ± 0.1 nm at 31 at.-% Zr, respectively. However, an increase of friction coefficient and RMS roughness (0.78, 26 ± 0.1 nm) is observed for the Cr-Zr-N film with the further increase of Zr content to 39 at.-% Zr and the wear resistance of the coating dropped significantly due to the random structure in the coatings.

Figure 6 shows the results of the scratch test against a 100 Cr6 steel ball for the sputtered Cr-N, Zr-N and Cr-Zr-N coatings with varying Zr contents. In this case, the wear on the counterface ball was observed under a scanning electron microscope and analysed by microanalysis X. The CrN film showed little damage to the ball which can be traced to the relatively low friction coefficient (0.55) in combination with their high hardness and Young's modulus (Fig. 6*a*), as reported earlier.[8,11,27] The chemical analysis showed that there is very low Cr or N concentration on the wear tracks as compared to the substrate elements and oxygen confirming that CrN has a good abrasive resistance.[8] For the Cr-N coating,

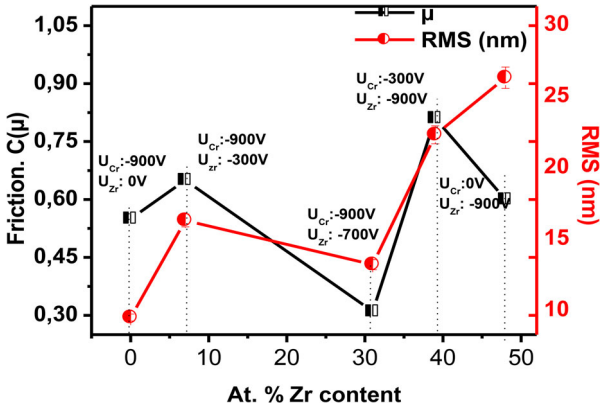

5 Friction coefficient and RMS roughness for Cr-N, Cr-Zr-N and Zr-N films

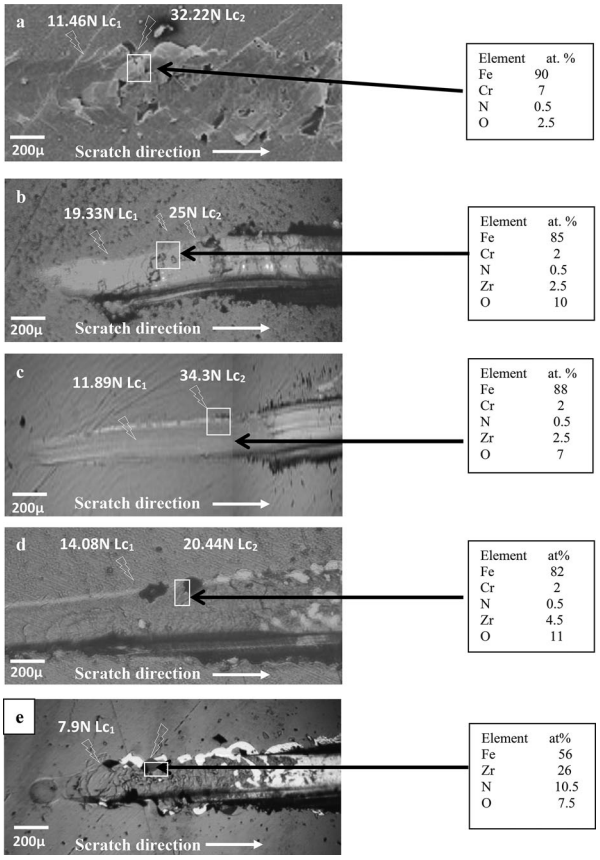

6 Scratch track micrographs for: *a* Cr-N, *b* Cr-Zr (7 at.-% Zr)-N, *c* Cr-Zr (31 at.-% Zr)-N, *d* Cr-Zr (39 at.-% Zr)-N and *e* Zr-N films

the cohesive and the adhesive failure critical loads are in the range of 11.46 and 32.2 N, respectively. These lower values as compared to the adhesion properties of Cr-N film[4,11,27] can be attributed to the presence of a high CrN residual stress film and a soft XC100 substrate.

Alloying of CrN with Zr showed a tendency to decrease the friction coefficient with increasing Zr content in the Cr-Zr-N film. The average friction coefficient at 31 at.-% Zr was measured to be approximately 0.42, which is lower than those of Cr-N and Zr-N films (Fig. 6*c*). In the first cycles of the wear track against a 100 Cr6 steel ball, smooth and abrasive type wear without any sign of debris adhesion was observed; also its wear rate was too negligible compared to Cr-N coating and in the dark regions of the wear track of Cr-Zr-N/100 Cr6, elements of the coating (Cr, Zr, N) and oxygen could be found. This excellent behaviour was observed also in Cr-Zr-N films deposited by closed field unbalanced magnetron sputtering against 100 Cr6 steel ball by Kim *et al.*,[3] which was attributed to its low surface roughness and high hardness. This behaviour is common in various metal-containing Cr-N systems. For example, addition of Ni to CrN coatings can significantly decrease the friction coefficient, especially in the bilayer Ni-Cr-N which showed a better interlayer adhesion and adhesion with mild steel substrate.[24] However, with adhesive critical high load of 34.3 N, delamination fracture of the Cr-Zr-N coating from the substrate was observed at the borders of the wear track (Fig. 6*c*). This fracture under high load conditions was mainly due to the ploughing action of wear debris.

However, at 39 at.-% of Zr, the adhesive failures occur at significantly lower critical load of 7 N (Fig. 6*d*). The chemical analysis showed that there are no coating elements on the adhesive wear tracks of Cr-Zr-N/100Cr6, and only Fe from the substrate and O were detected in the wear tracks. Thus, it appears that the addition of 39 at.-% Zr to the CrN system has a deterioration effect on the adhesion of the film. This may be explained by a reduction in the mechanical properties of the coating, especially the hardness and residual stress of the Cr–Zr–N system.

Concerning the Zr-N coating, a significant decrease of the Lc_1 was obtained (up to 7.9 N). The Zr-N film revealed a lower adhesive critical load of $Lc_2 \approx 14.5$ N. Nevertheless, from this applied load, a brittle failure mode was observed, as manifested by the formation of lateral cracks or chipping at the borders and the middle of the scratch tracks when the steel ball passed by (Fig. 6*e*). Gruss *et al.*[36] explained the formation of this type of crack by the influence of macro particles forming in the Zr-N film which act as stress raisers and cause the cracks to initiate. Also, these failures may originate from the lower thickness and the difference in the mechanical properties between the coating and substrate.

Conclusions

In this study the authors have presented structural, mechanical and tribological properties for five coating systems ranging from pure Cr-N through the various ternary alloys Cr-Zr-N compositions to pure Zr-N prepared onto Si and XC100 substrates by the R.F. reactive magnetron sputtering technique. The results revealed that:

- The deposited films showed a mixture of cubic and hexagonal phases with a columnar compact structure.
- The hardness and residual stress depends on the densification of the structure and low surface roughness.
- The maximum values of the hardness and residual stress due to the higher denseness, small grain size and preferred crystallite orientation are observed for the Cr-Zr-N coatings.
- The scratch tests showed that the wear resistance of Cr-Zr-N coatings was significantly improved in comparison to CrN film.
- Coefficient of friction and wear rate decreased with increasing Zr content and the best tribological properties were exhibited by the Cr-Zr-N coating at 31 at.-% Zr.

References

1. H. N. Shah, R. Jayaganthan and D. Kaur: *Surf. Eng.*, 2010, **26**, (8), 629–637.
2. M. Uchida, N. Nihira, A. Mitsuo, K. Toyoda, K. Kubota and T. Aizawa: *Surf. Coat. Technol.*, 2004, **177–178**, 627–630.
3. G. S. Kim, B. S. Kim, S. Y. Lee and J. H. Hahn: *Surf. Coat. Technol.*, 2005, **200**, 1669–1675.
4. X. Feng, H. Zhou, Z. Wan and K. Zhang: *Surf. Eng.*, 2017, **33**, (8), 619–625.
5. Q. M. Mehran, A. R. Bushroa and M. A. Fazal: *J. Adhesion Sci. Technol.*, 2015, **29**, (19), 2076–2089.
6. Y. Katoh, G. Vasudevamurthy, T. Nozawa and L. L. Snead: *J. Nucl. Mater.*, 2013, **441**, (1–3), 718–742.
7. C. Nouveau, M. A. Djouadi, P. Beer, M. Lambertin, C. Decès-Petit and P. L. Ko: *Ceramics*, 2000, **61**, 131–144.
8. L. Aissani, C. Nouveau, M. J. Walock, H. Djebaili and A. Djelloul: *Surf. Eng.*, 2015, **31**, (10), 779–788.
9. M. J. Twu, C. C. Hu, D. W. Liu, C. Y. Hsu and C. G. Kuo: *J. Exp. Nanosci.*, 2016, **11**, (7), 581–592.

10. S. K Pradhan, C. Nouveau, A. Vasin and M.-A. Djouadi: *Surf. Coat. Technol.*, 2005, **200**, 141–145.
11. J. W. Seok, N. M. Jadeed and R. Y. Lin: *Surf. Coat. Technol.*, 2001, **138**, (1), 14–22.
12. P. Hones, R. SanjineÂs and F. LeÂvy: *Thin Solid Films.*, 1998, **332**, 240–246.
13. C. Chantharangsi, S. Denchitcharoen, S. Chaiyakun and P. Limsuwan: *Proc. Eng.*, 2012, **32**, 868–874.
14. J. Pelleg, L. Z. Zevin, S. Lungo and N. Croitoru: *Thin Solid Films.*, 1991, **197**, 117–129.
15. U. C. Oh, J. H. Je and J. Y. Lee: *Mater. Res.*, 1995, **10**, 634–639.
16. A. Conde, A. B. Cristóbal, G. Fuentes, T. Tate and J. Damborenea: *Surf. Coat. Technol.*, 2006, **201**, 3588–3595.
17. H. C. Barshilia, N. Selvakumar, B. Deepthi and K. S. Rajam: *Surf. Coat. Technol.*, 2006, **201**, (6), 2193–2201.
18. B. Stypula and J. Stoch: *Corros. Sci.*, 1994, **36**, 2159–2167.
19. J. Lin, J. J. Moore, W. C. Moerbe, M. Pinkas, B. Mishra, G. L. Doll and W. D. Sproul: *Int. J. Refract. Met. Hard Mater.*, 2010, **28**, (1), 2–14.
20. M. D. Re, R. Gouttebaron, J. P. Dauchot, P. Leclère and M. Hecq: *Surf. Coat. Technol.*, 2003, **174–175**, 240–245.
21. T. Tański and K. Lukaszkowicz: *Surf. Eng.*, 2012, **28**, (8), 598–604.
22. S. M. Aouadi, T. Maeruf, R. D. Twesten, D. M. Mihut and S. L. Rohde: *Surf. Coat. Technol.*, 2006, **200**, 3411–3417.
23. S. Mahieu, P. Ghekiere, D. Depla and R. De Gryse: *Thin Solid Films.*, 2006, **515**, 1229–1249.
24. J. Bhatti, M. A. Fazal, A. F. Khan, A. R. Bushroa and M. M. Quazi: *J. Adhesion Sci. Technol.*, 2016, **30**, (20), 2224–2235.
25. W. Y. Yeung, S. N. Dub and R. Wuhrer: *Sci. Sintering.*, 2006, **38**, (3), 211–221.
26. R. Lamni, R. Sanjinés, M. Parlinska-Wojtan, A. Karimi and F. Lévy: *J. Vac. Sci. Technol. A.*, 2005, **23**, (4), 593–598ence.
27. K. Khlifi and A. Ben Cheikh Larbi: *Surf. Eng.*, 2013, **29**, (7), 555–560.
28. Y. P. Purandare, A. P. Ehiasarian, A. Santana and P. Eh Hovsepian: *J. Vac. Sci. Technol. A.*, 2014, **32**, (3), 031507.
29. R. W. Harris and W. E. Lee: *Adv. Appl. Ceram.: Struct., Funct. Bioceram.*, 2016, **115**, (5), 294–307.
30. C-S. Chen, C-P. Liu, C-Y. Tsao and H-G. Yan: *Scr. Mater.*, 2004, **51**, 715–719.
31. J. J. Zhang, M. X. Wang, J. Yang, Q. X. Liu and D. J. Li: *Surf. Coat. Technol.*, 2007, **201**, 5186–5189.
32. M. Pakala and R. Y. Lin: *Surf. Coat. Technol.*, 1996, **81**, 233–239.
33. D. H. Kim, T. F. Zhang, J. H. Shin, M. C. Kang and K. H. Kim: *Surf. Eng.*, 2016, **32**, (4), 4314–320.
34. K. E. Davies, B. K. Gan, D. R. Mc Kenzie, M. M. M. Bilek, M. B. Taylor, D. G. Mc Culloch and B. A. Latella: *J. Phys., Condens. Mater.*, 2004, **16**, (45), 7947–7954.
35. H-M. Tung, J-H. Huang, D-G. Tsai, C-F. Ai and G-P. Yu: *Mater. Sci. Eng. A.*, 2009, **500**, (1), 104–108.
36. K. A. Gruss and R. F. Davis: *Surf. Coat. Technol.*, 1999, **114**, 156–168.